

Enhanced model of load distribution along the line of contact for non-standard involute external gears

Miryam B. Sánchez · Miguel Pleguezuelos · José I. Pedrero

Received: 16 March 2012 / Accepted: 14 September 2012 / Published online: 9 October 2012
© Springer Science+Business Media Dordrecht 2012

Abstract The presence of undercut at the tooth root, non-equal addendum on pinion and wheel, non-standard tooth height or non-standard center distance may have decisive influence on the load distribution along the line of contact of spur and helical gear teeth. The curve of variation of the meshing stiffness along the path of contact, quite symmetric respect the midpoint of the interval of contact, loses its symmetry for non-standard geometries and operating conditions. As a consequence, the critical contact points for bending and wear calculations may be shifted from their locations for standard gears. In this paper, a non-uniform model of load distribution along the line of contact of standard spur and helical gears, obtained from the minimum elastic potential criterion, has been enhanced to fit with the meshing conditions of the above mentioned non-standard cylindrical gear pairs. The same analytical formulation of the initial model may be used for the non-standard gears by considering appropriate values of a virtual contact ratio, which are also presented in the paper.

Keywords Cylindrical gears · Gear geometry · Load distribution · Undercut teeth · Non-standard gears

Abbreviations

b	Face width, mm
C	Operating center distance, mm
d_α	Fractional part of ε_α
d_β	Fractional part of ε_β
E	Modulus of elasticity, MPa
e	Tooth chordal thickness, mm
F	Load, N
f	Load per unit of length, N/mm
G	Transverse modulus of elasticity, MPa
h_a	Addendum coefficient
h_{a0}	Tool addendum coefficient
m_n	Normal module, mm
R	Load sharing ratio
r_b	Base radius, mm
r_C	Contact point radius, mm
r_o	Outside radius, mm
r_p	Standard pitch radius, mm
U	Elastic potential, N mm
u	Unitary potential, mm^2/N
v	Inverse unitary potential, N/mm^2
x	Rack shift coefficient
y	Coordinate along the tooth centerline from the gear rotation center, mm
z	Number of teeth
α_C	Load angle
α_n	Standard normal pressure angle

M.B. Sánchez · M. Pleguezuelos · J.I. Pedrero (✉)
Departamento de Mecánica, UNED, Juan del Rosal 12,
28040 Madrid, Spain
e-mail: jpedrero@ind.uned.es

M.B. Sánchez
e-mail: msanchez@ind.uned.es

M. Pleguezuelos
e-mail: mpleguezuelos@ind.uned.es

α'_t	Operating transverse pressure angle (pressure angle at the pitch cylinder)
β	Standard helix angle
β_b	Base helix angle
ε_α	Transverse contact ratio
ε'_α	Fictitious transverse contact ratio
ε_β	Axial contact ratio (overlap ratio)
ξ	Involute profile parameter

1 Introduction

Calculation methods of spur and helical gears available in technical literature [1–3] use simple models of the theory of elasticity to evaluate the stress, assuming the load to be uniformly distributed along the line of contact. However, it is known that the load distribution depends on the meshing stiffness of the pair of teeth, which is different at any contact point, which means that the load per unit of length is also different at any point of the line of contact. For this reason, several influence factors for load distribution are introduced to correct the calculated values of the bending and contact stresses [1, 4].

Some studies on the load distribution along the line of contact can be found in technical literature [5–16], but all of them provide results obtained by numerical techniques or Finite Element Methods, presenting the problem of no generality of the obtained results: all of them allow to obtain some conclusions regarding the considered gear pairs, but make very difficult to extract general conclusions, valid for any gear pair.

In previous works [17, 18], the authors developed a new load distribution model from the minimum elastic potential energy criterion. The elastic potential energy of a pair of teeth was calculated and expressed as a function of the contact point and the normal load. The load sharing among several pairs of contacting teeth in spur gears was obtained by solving the variational problem of minimize the total potential energy (equal to the addition of the potential energy of each pair at its respective contact point) regarding the restriction of the total load to be equal to the sum of the load at each pair. The same approach was used for helical gear teeth by dividing each helical pair in infinite slices, perpendicular to the gear axis, assuming each slice to be equivalent to a spur gear with differential face width, and extending the integrals to the complete line of contact. This approach allowed the

value of the load per unit of length to be known at any point of the line of contact and at any position of the meshing cycle. Initially, numerical results obtained by the numerical integration of the equations of the elasticity were provided [17]. More recently, an analytic, approximate equation for the inverse unitary potential was presented [18], allowing to compute the load per unit of length at any point of the line of contact and at any position of the meshing cycle from the inverse unitary potential and its integral along the complete line of contact, which can be easily computed as the inverse unitary potential has now analytic expression. Undercut teeth were also considered [18]. From this model, some general studies on the load carrying capacity [19–21] and efficiency [22–24], were developed allowing to make new proposals for calculation methods, suitable for preliminary designs or standardization purposes.

An important conclusion of these studies was that the load distribution is very slightly affected by geometrical parameters as the number of teeth, the rack shift coefficients, the pressure angle, the tool tip radius or the helix angle. This allowed to express the inverse unitary potential (the inverse of elastic potential of the tooth pair for unit load and face width) as a function of only one parameter: the transverse contact ratio [18]. On the contrary, the load distribution is heavily affected by all the parameters having influence on the length of contact, as the tooth height, the operating center distance or the presence of vacuum gearing (reduction of the effective outside diameter due to the existence of undercut at the root of the meshing tooth).

In this paper, the same load distribution model of minimum elastic potential is extended to these cases of non-standard spur and helical gears, with non-standard values of the tooth height (including different values for pinion and wheel) or center distance. Additionally, the same formulation of the analytic, approximate equation for the inverse unitary potential is adjusted to fit to these non-standard gears by considering appropriate values of a fictitious transverse contact ratio.

2 Load distribution model

Reference [18] presents in detail the model of load distribution of minimum elastic potential energy. It is based on the assumption that the load distribution

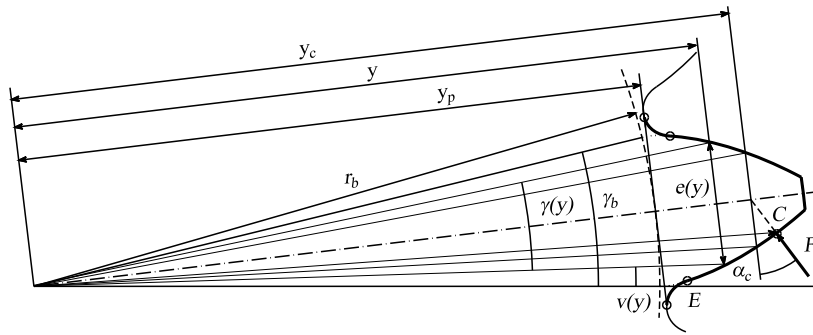


Fig. 1 Geometrical parameters of involute tooth

along the line of contact provides a minimum elastic potential energy. It has been obtained by computing the total elastic potential energy, considering all the pairs of teeth in simultaneous contact, with an unknown fraction of the load acting on each one, and minimizing its value by means of variational techniques. In this section, the model will be briefly described.

2.1 Background

The elastic potential energy of a spur tooth U can be expressed as the sum of the bending component U_x , the compressive component U_n and the shear component U_s :

$$U = U_x + U_n + U_s \tag{1}$$

All the components can be computed from the equations of the theory of elasticity and some geometrical parameters of the tooth which have been represented in Fig. 1. The application of those equations to the geometry of the involute teeth results in:

$$\begin{aligned} U_x &= 6 \frac{F^2 \cos^2 \alpha_C}{Eb} \int_{y_p}^{y_c} \frac{(y_c - y)^2}{e^3(y)} dy \\ U_n &= \frac{1}{2} \frac{F^2 \sin^2 \alpha_C}{Eb} \int_{y_p}^{y_c} \frac{dy}{e(y)} \\ U_s &= C \frac{1}{2} \frac{F^2 \cos^2 \alpha_C}{Gb} \int_{y_p}^{y_c} \frac{dy}{e(y)} \end{aligned} \tag{2}$$

where F is the normal load between both teeth, α_C the load angle, b the face width, E the modulus of elasticity of the material, G the transverse modulus of elasticity, and $e(y)$ the tooth chordal thickness at the section described by y , being y the coordinate along the tooth centerline from the gear rotation center.

y_p and y_C are the values of coordinate y corresponding to the encastred section (defined by the points of both sides of the profile at the root circle) and to the load section (defined by the intersection of the line of action of the load—i.e., the normal to the profile at the contact point—and the tooth centerline), respectively. Finally, C is the shear potential correction factor, which accounts the non-uniform distribution of the shear stresses on the section, according to the Colignon’s theorem. For rectangular section, this factor takes the value $C = 1.5$ [25].

To describe the contact point, the profile parameter ξ is defined as [17, 18]:

$$\xi = \frac{z}{2\pi} \sqrt{\frac{r_C^2}{r_b^2} - 1} \tag{3}$$

where z is the number of teeth, r_C the radius of the contact point and r_b the base radius. Note that the difference of ξ parameters corresponding to contact at the outer point of contact and at the inner point of contact is equal to the transverse contact ratio ϵ_α . Similarly, the difference of ξ parameters corresponding to two contiguous teeth in simultaneous contact is equal to 1.

According to this, the elastic potential energy of a tooth can be expressed as a function of the profile parameter of its load point (or contact point), $U = U(\xi)$. Of course, this is valid both for the pinion tooth and for the wheel tooth, so that:

$$\begin{aligned} U_1 &= U_1(\xi) \\ U_2 &= U_2(\xi_2) \end{aligned} \tag{4}$$

where subscripts 1 and 2 denote the pinion and the wheel, respectively (for simplicity, the pinion profile parameter will be denoted by ξ , without subscript). The sum of the curvature radii of both transverse profiles at the respective contact points is constant along

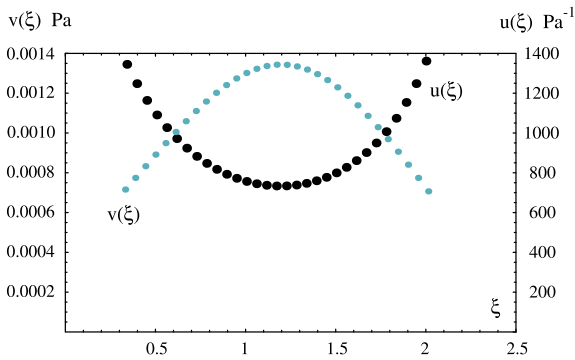


Fig. 2 Example of unitary potential u and inverse unitary potential v for spur gears (obtained by numerical integration)

the line of action, and equal to the distance between the tangency points of the operating pressure line and both base circles of pinion and wheel, which provides a relation between pinion and wheel profile parameters:

$$\xi + \xi_2 = \lambda = \frac{z_1 + z_2}{2\pi} \tan \alpha'_i \tag{5}$$

where α'_i is the operating transverse pressure angle (the pressure angle at the pitch cylinder) and λ the distance between both tangency points divided by the base radius and the angular pitch of the pinion. The potential energy of a pair of teeth in contact U_p will be the sum of those of the pinion and the wheel, which according to Eq. (5), may be expressed as a function of the pinion profile parameter ξ :

$$U_p = U_1 + U_2 = U_p(\xi) \tag{6}$$

Finally, two more parameters are defined [17, 18]: the unitary potential u , which is the elastic potential for unit load and face width, and the inverse unitary potential v , which is the inverse of u :

$$\begin{aligned} u(\xi) &= \frac{b}{F^2} U_p(\xi) \\ v(\xi) &= \frac{1}{u(\xi)} \end{aligned} \tag{7}$$

being F the load carried by the pair of teeth.

Both the unitary potential and the inverse unitary potential of a determined pair of teeth can be computed from the above equations by numerical techniques of integration. The result for standard teeth is always a function of ξ similar to that in Fig. 2.

2.2 Load distribution for spur gears

For spur gears, the elastic potential energy is computed considering all the pairs of teeth in simultaneous contact, with an unknown fraction of the load acting on each one, and minimizing its value by means of variational techniques (Lagrange’s method). The load at each pair results in [18]:

$$F_i(\xi_i) = \frac{v_i(\xi_i)}{\sum_{j=0}^{z_1-1} v_j(\xi_j)} F \tag{8}$$

where $F_i(\xi_i)$ and $v_i(\xi_i)$ are the load and the inverse unitary potential of tooth i when contact occurs at the point corresponding to ξ_i , F is the total transmitted load, and it is assumed $v_i(\xi_i) = 0$ outside the interval of contact $\xi_{inn} \leq \xi \leq \xi_{inn} + \varepsilon_\alpha$, where ξ_{inn} is the profile parameter corresponding to the inner contact point of the pinion. According to this, the load sharing ratio $R(\xi)$ (or the fraction of the load supported by the considered pair of teeth) is given by:

$$\begin{aligned} R_i(\xi_i) &= \frac{F_i(\xi_i)}{F} \\ &= \frac{v_i(\xi_i)}{\sum_{j=0}^{z_1-1} v_j(\xi_j)} \\ &= \frac{v(\xi_i)}{\sum_{j=0}^{z_1-1} v(\xi_i + (j - i))} \end{aligned} \tag{9}$$

while the load per unit of length $f(\xi)$, for spur gears, can be expressed as:

$$f_i(\xi_i) = \frac{F}{b} R_i(\xi_i) \tag{10}$$

2.3 Load distribution for helical gears

The same approach may be used for helical gears by dividing the helical tooth in infinite slices, perpendicular to the gear axis. Each slice is equivalent to a spur gear with differential face width. In this case, the difference between the ξ parameters of two slices separated a distance $d\delta$ along the gear axis (or dl along the line of contact) is [18]:

$$d\xi = \frac{\varepsilon_\beta}{b} d\delta = \frac{\varepsilon_\beta \cos \beta_b}{b} dl \tag{11}$$

where ε_β is the axial contact ratio (also known as overlap ratio [4]) and β_b the base helix angle. By following a similar method than that described for spur gears, the load per unit of length of a helical gear at a point of

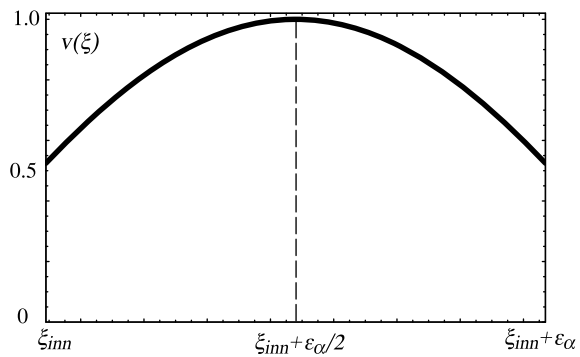


Fig. 3 Typical shape of the graph of inverse unitary potential $v(\xi)$

the line of contact described by ξ , at the meshing position corresponding to a reference transverse section contacting at point described by ξ_0 , results in [18]:

$$f(\xi, \xi_0) = \frac{\varepsilon_\beta \cos \beta_b}{b} \frac{v(\xi)}{I_v(\xi_0)} F \tag{12}$$

where function $I_v(\xi_0)$ is given by:

$$I_v(\xi_0) = \int_{l_c} v(\xi) d\xi = \sum_{j=0}^{z_1-1} \int_{\xi_0+j-\varepsilon_\beta}^{\xi_0+j} v(\xi) d\xi \tag{13}$$

The reference transverse section can be any arbitrary transverse section of the helical tooth, however the expression for $I_v(\xi_0)$ depends on the chosen section. The reference transverse section corresponding to Eq. (13) is the end section of the tooth with higher contact point on pinion.

2.4 Analytical approach

The inverse unitary potential $v(\xi)$ is described very accurately by the following approximate equation [18]:

$$v(\xi) = \cos[b_0(\xi - \xi_m)] \tag{14}$$

where:

$$\xi_m = \xi_{inn} + \frac{\varepsilon_\alpha}{2} \tag{15}$$

$$b_0 = \left[\frac{1}{2} \left(1 + \frac{\varepsilon_\alpha}{2} \right)^2 - 1 \right]^{-1/2}$$

Figure 3 shows the typical aspect of function $v(\xi)$ for standard teeth. Note that, according to Eqs. (9), (12) and (13), the amplitude of $v(\xi)$ has no influence on the load distribution, so a normalized function $v(\xi)$, with a maximum value equal to 1, may be considered

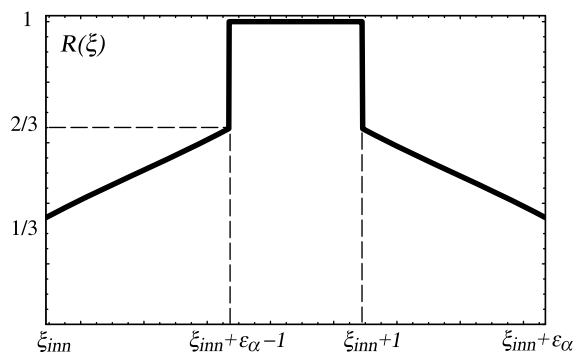


Fig. 4 Load sharing ratio for non-undercut spur gears (transverse contact ratio between 1 and 2)

for calculations, as one given by Eq. (14) and represented in Fig. 3. According to this, the load sharing ratio for spur gears can be obtained by replacing Eq. (14) in Eq. (9), which yields the following result for transverse contact ratio ε_α between 1 and 2:

$$R(\xi) = \frac{\cos[b_0(\xi - \xi_m)]}{\cos[b_0(\xi - \xi_m)] + \cos[b_0(\xi + 1 - \xi_m)]}$$

for $\xi_{inn} \leq \xi \leq \xi_{inn} + \varepsilon_\alpha - 1$

$$R(\xi) = 1$$

for $\xi_{inn} + \varepsilon_\alpha - 1 \leq \xi \leq \xi_{inn} + 1$

$$R(\xi) = \frac{\cos[b_0(\xi - \xi_m)]}{\cos[b_0(\xi - 1 - \xi_m)] + \cos[b_0(\xi - \xi_m)]}$$

for $\xi_{inn} + 1 \leq \xi \leq \xi_{inn} + \varepsilon_\alpha$

which has been represented in Fig. 4. The ordinates of singular points are always very close to 0.33 and 0.67, so that the load sharing ratio given by Eq. (16) can be also computed from:

$$R(\xi) = \frac{1}{3} \left(1 + \frac{\xi - \xi_{inn}}{\varepsilon_\alpha - 1} \right)$$

for $\xi_{inn} \leq \xi \leq \xi_{inn} + \varepsilon_\alpha - 1$

$$R(\xi) = 1$$

for $\xi_{inn} + \varepsilon_\alpha - 1 \leq \xi \leq \xi_{inn} + 1$

$$R(\xi) = \frac{1}{3} \left(1 + \frac{\xi_{inn} + \varepsilon_\alpha - \xi}{\varepsilon_\alpha - 1} \right)$$

for $\xi_{inn} + 1 \leq \xi \leq \xi_{inn} + \varepsilon_\alpha$

For helical gears, the load per unit of length at any contact point (described by ξ) at any meshing position (described by ξ_0) is given by Eq. (12), in which $v(\xi)$ and $I_v(\xi_0)$ are given by Eqs. (14) and (13), respectively. Another equation for $I_v(\xi_0)$ more explicit than Eq. (13) can be found in [18]. Function $I_v(\xi_0)$

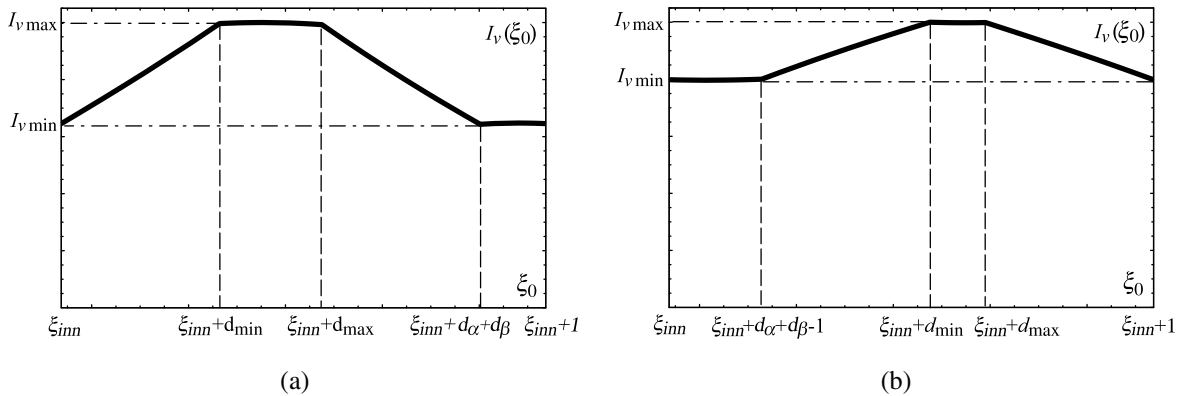


Fig. 5 Typical shapes of the graphs of function $I_v(\xi_0)$: **(a)** $d_\alpha + d_\beta < 1$; **(b)** $d_\alpha + d_\beta > 1$

takes different shapes depending on whether the sum of the fractional parts of both transverse and axial contact ratios (d_α and d_β , respectively) is less than 1 or not, as represented in Fig. 5.

3 Non-standard gears

As concluded in [18], neither the geometrical parameters (as the numbers of teeth, the rack shift coefficients, the pressure angle, the helix angle, etc.) nor the operating parameters (as the operating pressure angle or the operating center distance) have significant influence on the load distribution. In fact, according to Eq. (17) and Fig. 4, the load sharing ratio of spur gears only depends on the contact ratio ε_α and the pinion profile parameter at the inner point of contact ξ_{inn} . This made possible to express the inverse unitary potential $v(\xi)$ as a function of the same two parameters, as shown in Eqs. (14) and (15). However, in all the cases considered in the developed study of accuracy [18], the tooth addendum was kept equal to the normal module m_n , the tooth dedendum $1.25m_n$ and the outside diameter taken according to the operating center distance in such a way that the distance between the outside circle of one gear and the root circle of the mating gear was equal to $0.25m_n$.

The same study [18] revealed that the existence of undercut has no influence on the load distribution, except if the undercut area is big enough to cause the outer points of the wheel profile not to find active profile on pinion to mesh with, as represented in Fig. 6. This is what is called vacuum gearing.

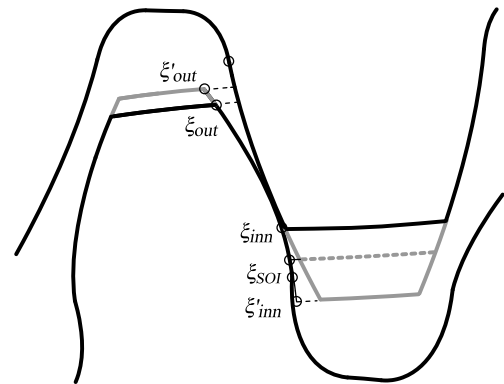


Fig. 6 Vacuum gearing

If vacuum gearing exists, the effective outside diameter of the wheel is smaller than the real one, but according to Eqs. (2) and Fig. 1, the integrals to compute the elastic potential are exactly the same, with the only difference that contact does not exist between the inner point of contact ξ_{inn} and the fictitious inner point of contact ξ'_{inn} (the fictitious point of the pinion profile that would mesh with the real outer point of the wheel, which can be obtained from Eq. (5)). This means that the values of the inverse unitary potential $v(\xi)$ of the undercut gear pair will be the same as those for the fictitious non-undercut gear pair, except in the interval $[\xi'_{inn}, \xi_{inn}]$, as represented in Figs. 7(a) and 7(b).

3.1 Reduced tooth height

It is obvious that the existence of vacuum gearing at the pinion root has the same effect on the load distribution as a reduction of the addendum on the wheel

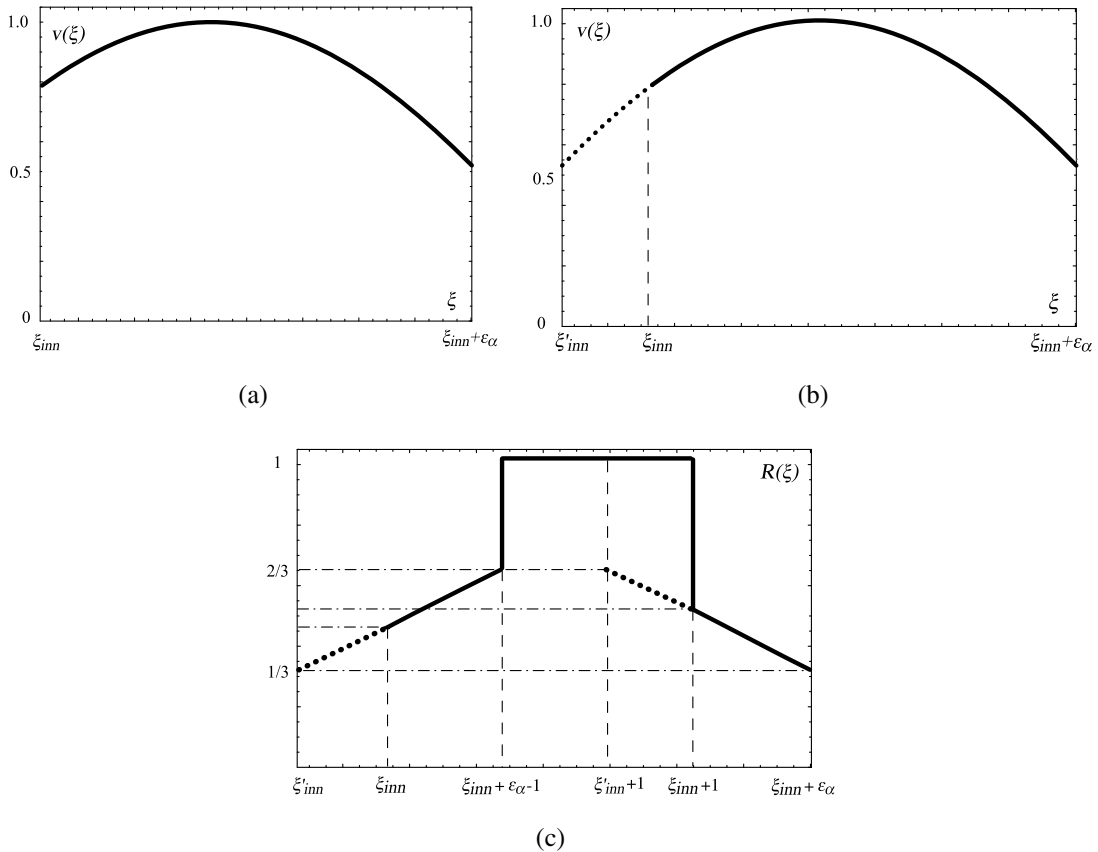


Fig. 7 Vacuum gearing transmissions: (a) inverse unitary potential by numerical integration of the equations of elasticity; (b) inverse unitary potential by truncated approximate cosine function; (c) load sharing ratio

tooth, as shown in Fig. 6. The integrals (2) are exactly the same, and the domain of contact is exactly the same too. Consequently, both for vacuum gearing at pinion root or reduced addendum on the wheel, the inverse unitary potential, represented in Figs. 7(a) and 7(b), is described by:

$$\begin{aligned}
 v(\xi) &= \cos[b'_0(\xi - \xi'_m)] \\
 &\text{for } \xi_{inn} \leq \xi \leq \xi_{inn} + \epsilon_\alpha \\
 v(\xi) &= 0 \\
 &\text{for } \xi < \xi_{inn} \text{ or } \xi > \xi_{inn} + \epsilon_\alpha
 \end{aligned}
 \tag{18}$$

where:

$$\begin{aligned}
 \xi'_m &= \xi'_{inn} + \frac{\epsilon'_\alpha}{2} \\
 b'_0 &= \left[\frac{1}{2} \left(1 + \frac{\epsilon'_\alpha}{2} \right)^2 - 1 \right]^{-1/2} \\
 \epsilon'_\alpha &= \epsilon_\alpha + (\Delta\epsilon_\alpha)_{inn} = \epsilon_\alpha + (\xi_{inn} - \xi'_{inn})
 \end{aligned}
 \tag{19}$$

ϵ'_α is the fictitious transverse contact ratio, and corresponds to the fictitious standard gear pair with non-reduced effective addendum.

For spur gears, the load sharing ratio for reduced effective addendum on the wheel is represented in Fig. 7(c). Its values can be computed from Eqs. (9), (18) and (19), but good approximations can be also obtained from:

$$\begin{aligned}
 R(\xi) &= \frac{1}{3} \left(1 + \frac{\xi - \xi'_{inn}}{\epsilon'_\alpha - 1} \right) \\
 &\text{for } \xi_{inn} \leq \xi \leq \xi_{inn} + \epsilon_\alpha - 1 \\
 R(\xi) &= 1 \\
 &\text{for } \xi_{inn} + \epsilon_\alpha - 1 \leq \xi \leq \xi_{inn} + 1 \\
 R(\xi) &= \frac{1}{3} \left(1 + \frac{\xi'_{inn} + \epsilon'_\alpha - \xi}{\epsilon'_\alpha - 1} \right) \\
 &\text{for } \xi_{inn} + 1 \leq \xi \leq \xi_{inn} + \epsilon_\alpha
 \end{aligned}
 \tag{20}$$

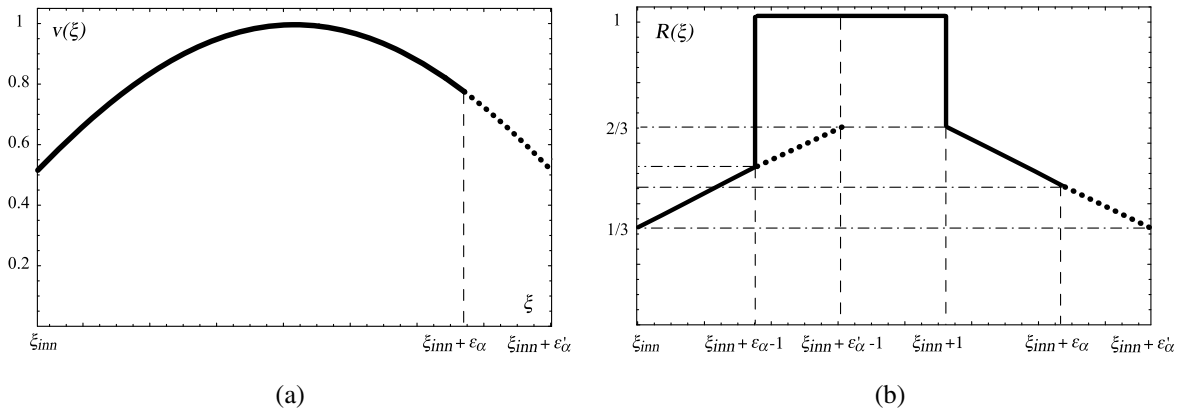


Fig. 8 Reduced effective addendum on pinion: **(a)** inverse unitary potential; **(b)** load sharing ratio

For helical gears, the load per unit of length may be computed from Eqs. (12), (13), (18) and (19). As for standard gears, function $I_v(\xi_0)$ takes different shapes depending on whether the sum of the fractional parts of both transverse and axial contact ratios is less than 1 or not, and its graphic representations are equal to those in Fig. 5. Another equation for $I_v(\xi_0)$ more explicit than Eq. (13) for gears with reduced effective addendum on the wheel can be found in [21].

Equation (18) remains valid for reduced effective addendum on the pinion, but in this case, according to Fig. 8(a):

$$\begin{aligned} \xi'_m &= \xi_{inn} + \frac{\varepsilon'_\alpha}{2} \\ b'_0 &= \left[\frac{1}{2} \left(1 + \frac{\varepsilon'_\alpha}{2} \right)^2 - 1 \right]^{-1/2} \\ \varepsilon'_\alpha &= \varepsilon_\alpha + (\Delta\varepsilon_\alpha)_{out} = \varepsilon_\alpha + (\xi'_{out} - \xi_{out}) \end{aligned} \tag{21}$$

where ξ'_{out} is the profile parameter of the fictitious outer point of contact of the pinion (corresponding to the non-reduced outer point of the pinion profile) and ξ_{out} the profile parameter of the actual outer point of contact of the pinion (considering addendum reduction or vacuum gearing at wheel tooth root).

For spur gears, the load sharing ratio for reduced effective addendum on the pinion can be computed from Eqs. (9), (18) and (21). Also in this case, a good approximation can be obtained from:

$$\begin{aligned} R(\xi) &= \frac{1}{3} \left(1 + \frac{\xi - \xi_{inn}}{\varepsilon'_\alpha - 1} \right) && \text{for } \xi_{inn} \leq \xi \leq \xi_{inn} + \varepsilon_\alpha - 1 \\ R(\xi) &= 1 && \text{for } \xi_{inn} + \varepsilon_\alpha - 1 \leq \xi \leq \xi_{inn} + 1 \\ R(\xi) &= \frac{1}{3} \left(1 + \frac{\xi_{inn} + \varepsilon'_\alpha - \xi}{\varepsilon'_\alpha - 1} \right) && \text{for } \xi_{inn} + 1 \leq \xi \leq \xi_{inn} + \varepsilon_\alpha \end{aligned} \tag{22}$$

Figure 8(b) represents the load sharing ratio for reduced effective addendum on the pinion.

Once again, for helical gears, the load per unit of length may be computed from Eqs. (12), (13), (18) and (21), and function $I_v(\xi_0)$ takes the same different shapes depending on whether the sum of the fractional parts of both transverse and axial contact ratios is less than 1 or not.

The same approach can be used for reduced effective addendum in both gears, even for different reductions on pinion and wheel. According to Fig. 9(a), the inverse unitary potential will be given by Eq. (18), with:

$$\begin{aligned} \xi'_m &= \xi'_{inn} + \frac{\varepsilon'_\alpha}{2} \\ b'_0 &= \left[\frac{1}{2} \left(1 + \frac{\varepsilon'_\alpha}{2} \right)^2 - 1 \right]^{-1/2} \\ \varepsilon'_\alpha &= \varepsilon_\alpha + (\Delta\varepsilon_\alpha)_{inn} + (\Delta\varepsilon_\alpha)_{out} \\ &= \varepsilon_\alpha + (\xi_{inn} - \xi'_{inn}) + (\xi'_{out} - \xi_{out}) \end{aligned} \tag{23}$$

The load sharing ratio for spur gears will be:

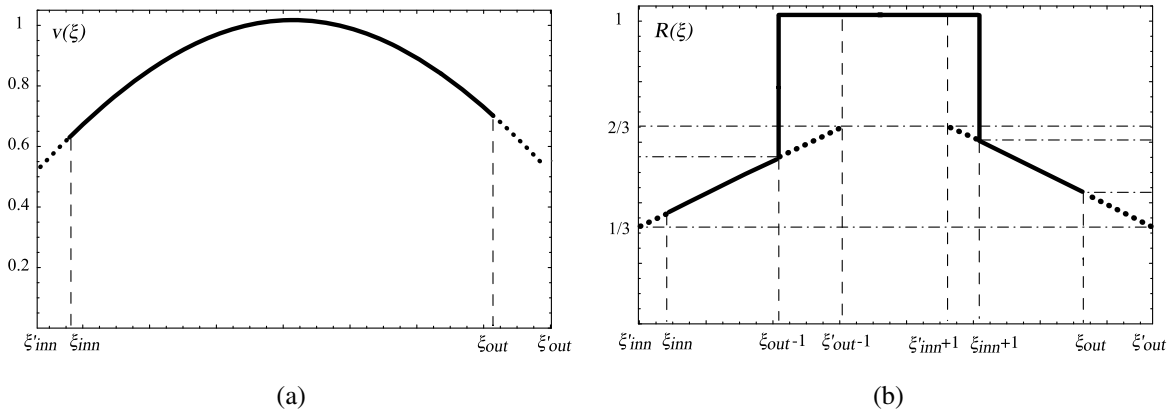


Fig. 9 Reduced effective addendum on pinion and wheel: (a) inverse unitary potential; (b) load sharing ratio

$$\begin{aligned}
 R(\xi) &= \frac{1}{3} \left(1 + \frac{\xi - \xi'_{inn}}{\varepsilon'_\alpha - 1} \right) \\
 &\text{for } \xi_{inn} \leq \xi \leq \xi_{inn} + \varepsilon_\alpha - 1 \\
 R(\xi) &= 1 \\
 &\text{for } \xi_{inn} + \varepsilon_\alpha - 1 \leq \xi \leq \xi_{inn} + 1 \\
 R(\xi) &= \frac{1}{3} \left(1 + \frac{\xi'_{inn} + \varepsilon'_\alpha - \xi}{\varepsilon'_\alpha - 1} \right) \\
 &\text{for } \xi_{inn} + 1 \leq \xi \leq \xi'_{inn} + \varepsilon_\alpha
 \end{aligned}
 \tag{24}$$

while for helical gears, the load per unit of length may be computed from Eqs. (12), (13), (18) and (23), as in the previous cases. Function $R(\xi)$ has been represented in Fig. 9(b).

Reduced dedendum on pinion or wheel has very small influence on the load distribution, as well as the influence of the tool tip radius is very small too. This is due to dedendum modifications have no influence neither on the inner point of contact parameter ξ_{inn} nor on the transverse contact ratio ε_α . Obviously, the interference restriction should be regarded.

3.2 Enlarged tooth height

Enlarged addendum can be also taken into account in a similar way. Equations (18) and (23) remain valid, with the only difference that $(\Delta\varepsilon_\alpha)_{inn}$ and $(\Delta\varepsilon_\alpha)_{out}$ are now negative, as seen in Figs. 6 and 10. Of course, Eq. (24) for spur gears and Eqs. (12) and (13) for helical gears, remain valid too.

Similarly, gear pairs with enlarged addendum in one gear and reduced addendum in the other gear can be studied with the same equations, considering one $(\Delta\varepsilon_\alpha)$ positive, and negative the other one. Figure 11

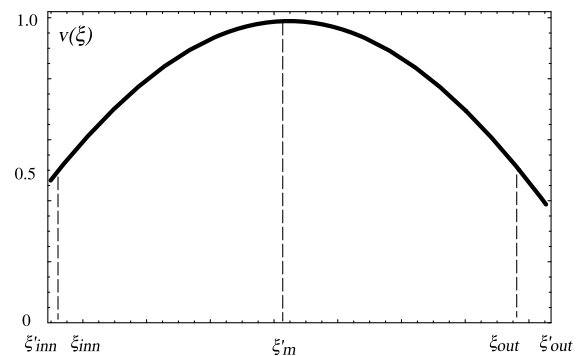


Fig. 10 Inverse unitary potential for enlarged effective addendum on pinion and wheel

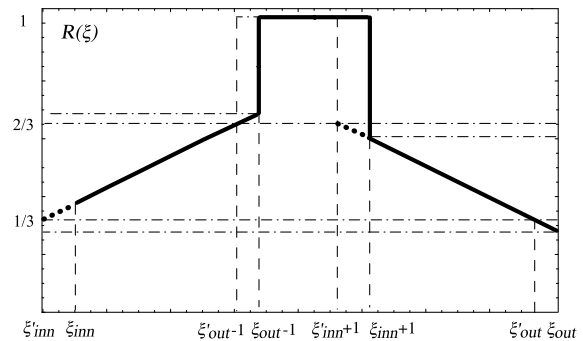


Fig. 11 Load sharing ratio for enlarged addendum on pinion and reduced addendum on wheel

shows the load sharing ratio of a spur gear pair with enlarged addendum on the pinion and reduced dedendum on the wheel.

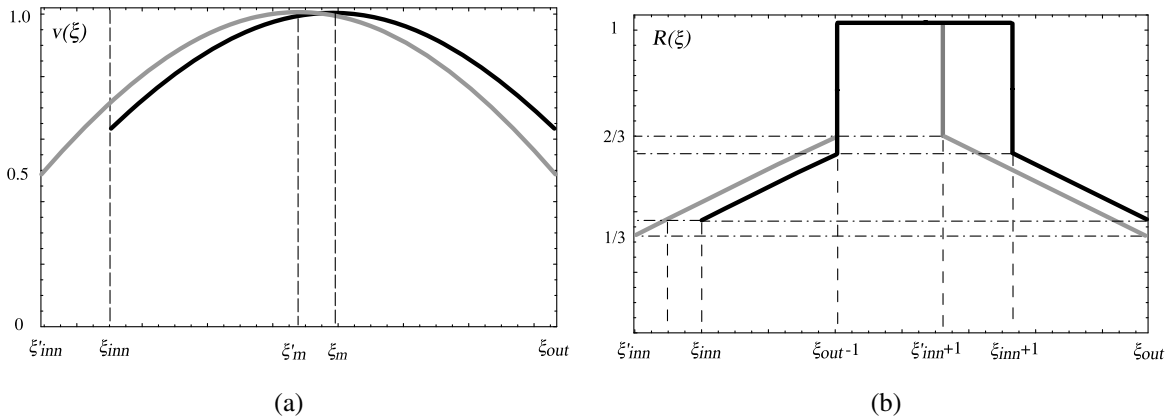


Fig. 12 Increased operating center distance: (a) inverse unitary potential; (b) load sharing ratio

3.3 Center distance modifications

To keep the radial clearance for non-standard center distance, the outside radii should be computed from:

$$\begin{aligned} r_{o1} &= C - r_{p2} - m_n x_2 + m_n h_a \\ r_{o2} &= C - r_{p1} - m_n x_1 + m_n h_a \end{aligned} \tag{25}$$

where r_o is the outside radius, C the operating center distance, r_p the standard pitch radius, x the rack shift coefficient and h_a the addendum coefficient. With these outside radii, the center distance has a slight influence on the transverse contact ratio, and Eqs. (14) and (15)—also Eq. (17) for spur gears—are valid if h_a is equal to 1.

Nevertheless, center distance modifications have strong influence on the transverse contact ratio if the outside radii are kept unalterable. In this case, these variations of the transverse contact ratio have influence on the load distribution in a similar way as tooth height modifications have.

An increase on the center distance means a decrease on the transverse contact ratio, which will be denoted by $(\Delta\varepsilon_\alpha)_c$. Since each addendum circles are moved away from the root circle of the mating gear, the effect of the increase on the center distance is equivalent to a reduction on both addendum circles. Consequently, the curve of the inverse unitary potential $v(\xi)$ should be truncated at both sides an amount of $0.5 \cdot (\Delta\varepsilon_\alpha)_c$. However, the profile parameter of the outer point of the pinion ξ_o does not change, because it depends on the outside radius but not on the center distance, as shown in Eq. (3). So that, the function $v(\xi)$ should be shifted to the right the same amount

of $0.5 \cdot (\Delta\varepsilon_\alpha)_c$, to get its final form as represented in Fig. 12(a). According to this, the inverse unitary potential will be described once again by:

$$\begin{aligned} v(\xi) &= \cos[b'_0(\xi - \xi_m)] \\ &\text{for } \xi_{inn} \leq \xi \leq \xi_{inn} + \varepsilon_\alpha \\ v(\xi) &= 0 \\ &\text{for } \xi < \xi_{inn} \text{ or } \xi > \xi_{inn} + \varepsilon_\alpha \end{aligned} \tag{26}$$

with:

$$\begin{aligned} \xi_m &= \xi_{inn} + \frac{\varepsilon_\alpha}{2} \\ b'_0 &= \left[\frac{1}{2} \left(1 + \frac{\varepsilon'_\alpha}{2} \right)^2 - 1 \right]^{-1/2} \\ \varepsilon'_\alpha &= \varepsilon_\alpha + (\Delta\varepsilon_\alpha)_c \end{aligned} \tag{27}$$

For spur gears, the load sharing ratio is given by:

$$\begin{aligned} R(\xi) &= \frac{1}{3} \left(1 + \frac{\xi - \xi_{inn} + 0.5(\Delta\varepsilon_\alpha)_c}{\varepsilon'_\alpha - 1} \right) \\ &\text{for } \xi_{inn} \leq \xi \leq \xi_{inn} + \varepsilon_\alpha - 1 \\ R(\xi) &= 1 \\ &\text{for } \xi_{inn} + \varepsilon_\alpha - 1 \leq \xi \leq \xi_{inn} + 1 \\ R(\xi) &= \frac{1}{3} \left(1 + \frac{\xi'_{inn} + \varepsilon_\alpha + 0.5(\Delta\varepsilon_\alpha)_c - \xi}{\varepsilon'_\alpha - 1} \right) \\ &\text{for } \xi_{inn} + 1 \leq \xi \leq \xi_{inn} + \varepsilon_\alpha \end{aligned} \tag{28}$$

which has been represented in Fig. 12(b). For helical gears, the load per unit of length can be computed from Eqs. (12), (13), (26) and (27).

Obviously, Eqs. (26), (27) and (28) are also valid for decreased center distance by taking negative values of the variation of the transverse contact ratio $(\Delta\varepsilon_\alpha)_c$.

4 Accuracy of the method

To check the accuracy of the above equations a set of studies has been carried out. Each study includes 20 different cases corresponding to the combination of 5 values of the pressure angle α_n (17, 19, 21, 23 and 25 deg) with 4 values of the gear ratio u (1.1, 2, 3 and 4). The number of teeth on pinion is different for each pressure angle (30 teeth for 17 and 19 deg pressure angle, 25 teeth for 21 deg, 20 teeth for 23 deg and 18 teeth for 25 deg), while the helix angle β and the rack shift coefficients x_1 and x_2 are all kept constant and equal to 0.

For every one of the 20 cases of each study, functions $v(\xi)$ and $R(\xi)$ computed by numerical integration of the equations of the elasticity have been compared with the same functions computed from the equations presented in Sect. 3. As normalized values of $v(\xi)$ have been used ($v_{max} = 1$) errors at points close to the midpoint of the interval of contact will be necessarily small, while errors at the limits of the interval of contact, ξ_{inn} and $\xi_{out} = \xi_{inn} + \varepsilon_\alpha$, will be more significant. Table 1 presents, for each study, the maximum relative error in the estimation of $v(\xi)$ at the limits of the interval of contact (corresponding to the 20 cases of the considered study) as well as the absolute maximum in the whole interval (the greater maximum error of the 20 cases). The location of the absolute maximum error in the interval of contact is also given and described by:

$$\delta = \frac{\xi - \xi_{inn}}{\xi_{out} - \xi_{inn}} \tag{29}$$

The adjusted R^2 -factor has been also computed for the 20 cases of each study; Table 1 presents the best one and the worst. In all the cases, the data (pressure angle and gear ratio) corresponding to each maximum or minimum, are given.

Table 1 also presents the maximum relative error in the estimation of $R(\xi)$ at the limits of the interval of contact, as well as the absolute maximum error and its location in the contact interval. The load sharing ratio, for spur gears with contact ratio between 1 and 2, is equal to 1 along the interval of one pair tooth contact, at the middle of the interval of contact, so the maximum relative error in the estimation of $R(\xi)$ will be located in or close to the contact interval limits. The best and the worst R^2 -factors are also presented.

Study_0 is a reference study developed with standard transmissions, with addendum coefficient $h_a =$

1.00, tool addendum coefficient $h_{a0} = 1.25$ and center distance $C = r_{p1} + r_{p2}$. This study does not provide new results with respect to the results presented in [17] and [18], but it has been carried out with the same 20 transmissions in order to compare the range of deviations.

As seen in Table 1, the maximum error in the estimation of the inverse unitary potential $v(\xi)$ was 7.25 %, and it was obtained for the case with minimum pressure angle ($\alpha_n = 17^\circ$) and maximum gear ratio ($u = 4$). This is also the case providing the worse fit between the numerically computed function and the approximate equation of $v(\xi)$; however, the obtained R^2 factor of 0.9820 is good enough for calculations. The best fit was obtained for maximum pressure angle ($\alpha_n = 25^\circ$) and minimum gear ratio ($u = 1.1$), with R^2 factor of 0.9995. Numerical and analytical functions of $v(\xi)$ for both best-fit and worst-fit cases have been represented in Fig. 13.

Even better results are obtained in the estimation of the load sharing ratio $R(\xi)$. The maximum error was 4.40 % and was obtained for the same case of maximum error in $v(\xi)$ but at a different contact point ($\delta = 0.12$ instead of 0.18). Smallest R^2 factor was also obtained for this case, but its value increased to 0.9910. Highest R^2 factor corresponded to the same case for $v(\xi)$, but its value increased in this case up to 0.9999. Figure 14 represents the numerical and the analytical functions of $R(\xi)$ for these cases of maximum and minimum R^2 factor.

Study_1a and Study_1b consider reduced tooth height on pinion, a 10 % reduction in the first one ($h_{a1} = 0.9$) and a 20 % ($h_{a1} = 0.8$) in the second. As shown in Table 1, variations of the maximum error of $v(\xi)$ are not significant. Variations of maximum error of $R(\xi)$ are very small as well. Moreover, errors at the inner point of the interval of contact are even smaller, which is expectable as divergences tend to increase as the limit points are far from the midpoint of the interval of contact. Maximum and minimum values of the R^2 factor of $v(\xi)$ and $R(\xi)$ curves are more or less the same as those for standard transmissions, keeping good enough fit levels, slightly better for the worst-fit curve of the load sharing ratio even.

Study_1c and Study_1d, which consider 10 % and 20 % reduced addendum on wheel, show very similar tendencies: very small variations of the maximum errors of $v(\xi)$ and $R(\xi)$ —around 7.25 % and 4.4 %, respectively—and similar values of the R^2 factor, higher than 0.99 for all the cases. Errors decrease

Table 1 Results of the studies of accuracy

Study	Error $v(\xi)$			Adjusted $R^2[v(\xi)]$			Error $R(\xi)$			Adjusted $R^2[R(\xi)]$		
	ξ_{inn} (α_n, u)	ξ_{out} (α_n, u)	$\xi_{max\ err}$ (α_n, u, δ)	max (α_n, u)	min (α_n, u)	ξ_{inn} (α_n, u)	ξ_{out} (α_n, u)	$\xi_{max\ err}$ (α_n, u, δ)	max (α_n, u)	min (α_n, u)		
Study_0 (Standard)	6.78 % (25°, 1.1)	6.45 % (25°, 1.1)	7.25 % (17°, 4.0, 0.160)	0.9995 (25°, 1.1)	0.9820 (17°, 4.0)	4.30 % (25°, 1.1)	4.14 % (25°, 1.1)	4.40 % (17°, 4.0, 0.120)	0.9999 (19°, 1.1)	0.9910 (17°, 4.0)		
Study_1a ($h_{a1} = 0.9$)	6.65 % (25°, 1.1)	4.22 % (25°, 1.1)	7.29 % (17°, 4.0, 0.165)	0.9995 (25°, 1.1)	0.9800 (17°, 4.0)	4.20 % (25°, 1.1)	2.46 % (25°, 1.1)	4.44 % (17°, 4.0, 0.135)	0.9999 (19°, 1.1)	0.9952 (17°, 4.0)		
Study_1b ($h_{a1} = 0.8$)	6.54 % (25°, 1.1)	2.65 % (25°, 1.1)	7.34 % (17°, 4.0, 0.170)	0.9995 (25°, 1.1)	0.9784 (17°, 4.0)	4.10 % (25°, 1.1)	1.27 % (25°, 1.1)	4.47 % (17°, 4.0, 0.140)	0.9999 (21°, 1.1)	0.9953 (17°, 4.0)		
Study_1c ($h_{a2} = 0.9$)	4.53 % (17°, 4.0)	6.34 % (25°, 1.1)	7.24 % (25°, 1.1, 0.113)	0.9996 (25°, 1.1)	0.9787 (17°, 4.0)	3.10 % (17°, 4.0)	4.05 % (25°, 1.1)	4.40 % (25°, 4.0, 0.083)	0.9999 (19°, 1.1)	0.9944 (17°, 4.0)		
Study_1d ($h_{a2} = 0.8$)	6.59 % (17°, 4.0)	6.24 % (25°, 1.1)	7.23 % (25°, 4.0, 0.063)	0.9995 (25°, 1.1)	0.9757 (17°, 4.0)	4.26 % (17°, 4.0)	3.97 % (25°, 4.0)	4.39 % (25°, 4.0, 0.030)	0.9999 (19°, 1.1)	0.9967 (17°, 4.0)		
Study_2a ($h_{a1} = 1.05$)	6.84 % (25°, 1.1)	7.80 % (25°, 1.1)	7.80 % (25°, 1.1, 1.000)	0.9995 (25°, 1.1)	0.9826 (17°, 4.0)	4.35 % (25°, 1.1)	5.20 % (25°, 1.1)	5.20 % (25°, 1.1, 1.000)	0.9999 (25°, 3.0)	0.9875 (17°, 4.0)		
Study_2b ($h_{a1} = 1.1$)	6.90 % (25°, 1.1)	9.30 % (25°, 1.1)	9.30 % (25°, 1.1, 1.000)	0.9995 (25°, 1.1)	0.9888 (19°, 4.0)	4.40 % (25°, 1.1)	6.42 % (25°, 1.1)	6.42 % (25°, 1.1, 1.000)	0.9999 (25°, 3.0)	0.9963 (17°, 2.0)		
Study_2c ($h_{a2} = 1.05$)	8.31 % (25°, 1.1)	6.50 % (25°, 1.1)	8.31 % (25°, 4.0, 0.000)	0.9995 (25°, 1.1)	0.9861 (17°, 3.0)	5.50 % (25°, 1.1)	4.18 % (25°, 1.1)	5.50 % (25°, 1.1, 0.000)	0.9999 (19°, 1.1)	0.9919 (17°, 3.0)		
Study_2d ($h_{a2} = 1.1$)	10.05 % (25°, 1.1)	6.55 % (25°, 1.1)	10.05 % (25°, 1.1, 0.000)	0.9994 (25°, 1.1)	0.9874 (19°, 4.0)	6.91 % (25°, 1.1)	4.22 % (25°, 1.1)	6.91 % (25°, 1.1, 0.000)	0.9997 (19°, 1.1)	0.9954 (17°, 2.0)		
Study_2e ($h_{a1} = 1.1, h_{a2} = 1.05$)	8.44 % (25°, 1.1)	9.36 % (25°, 1.1)	9.36 % (25°, 1.1, 1.000)	0.9995 (25°, 1.1)	0.9890 (19°, 4.0)	5.61 % (25°, 1.1)	6.47 % (25°, 1.1)	6.47 % (25°, 1.1, 1.000)	0.9998 (25°, 4.0)	0.9960 (19°, 4.0)		
Study_3a ($h_{a01} = 1.2$)	5.30 % (25°, 1.1)	6.65 % (25°, 1.1)	8.79 % (17°, 4.0, 0.150)	0.9984 (25°, 1.1)	0.9710 (17°, 4.0)	3.08 % (25°, 1.1)	4.65 % (25°, 1.1)	5.56 % (17°, 4.0, 0.127)	0.9997 (21°, 1.1)	0.9840 (17°, 4.0)		
Study_3b ($h_{a01} = 1.3$)	8.23 % (25°, 1.1)	6.23 % (25°, 1.1)	8.23 % (25°, 1.1, 0.000)	0.9985 (25°, 1.1)	0.9893 (17°, 4.0)	5.50 % (25°, 1.1)	3.61 % (25°, 1.1)	5.50 % (25°, 1.1, 0.000)	0.9999 (several)	0.9955 (17°, 4.0)		
Study_4 ($C = r_{p1} + r_{p2} + 0.05m_n$)	3.98 % (19°, 4.0)	5.71 % (25°, 4.0)	7.50 % (17°, 4.0, 0.130)	0.9995 (25°, 1.1)	0.9852 (17°, 4.0)	2.70 % (19°, 4.0)	2.24 % (19°, 4.0)	4.40 % (17°, 4.0, 0.093)	1.0000 (23°, 1.1)	0.9954 (17°, 4.0)		

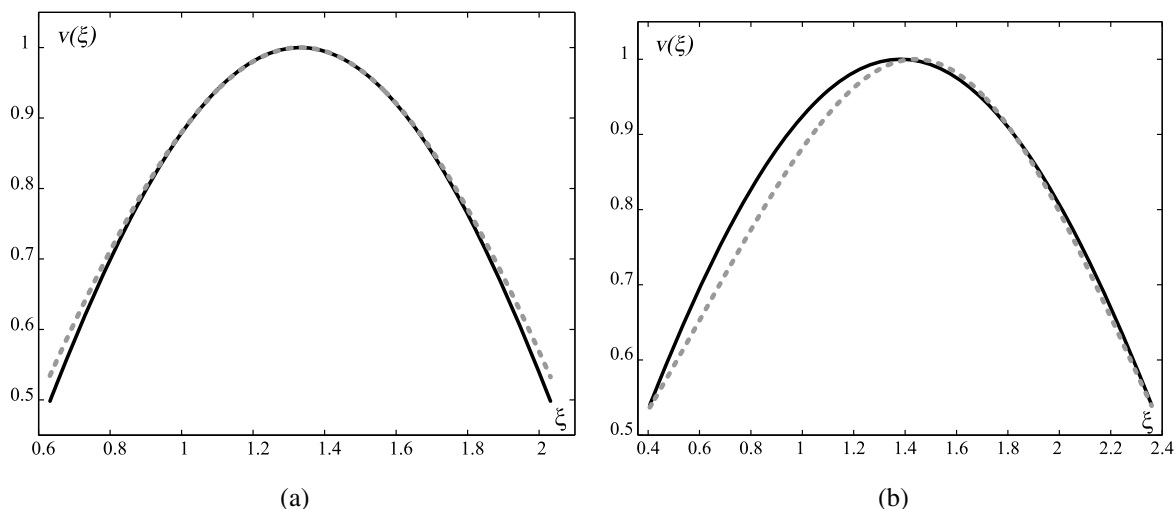


Fig. 13 Fit between numerical (*dashed*) and analytical (*solid*) functions of $v(\xi)$: (a) best fit; (b) worst fit

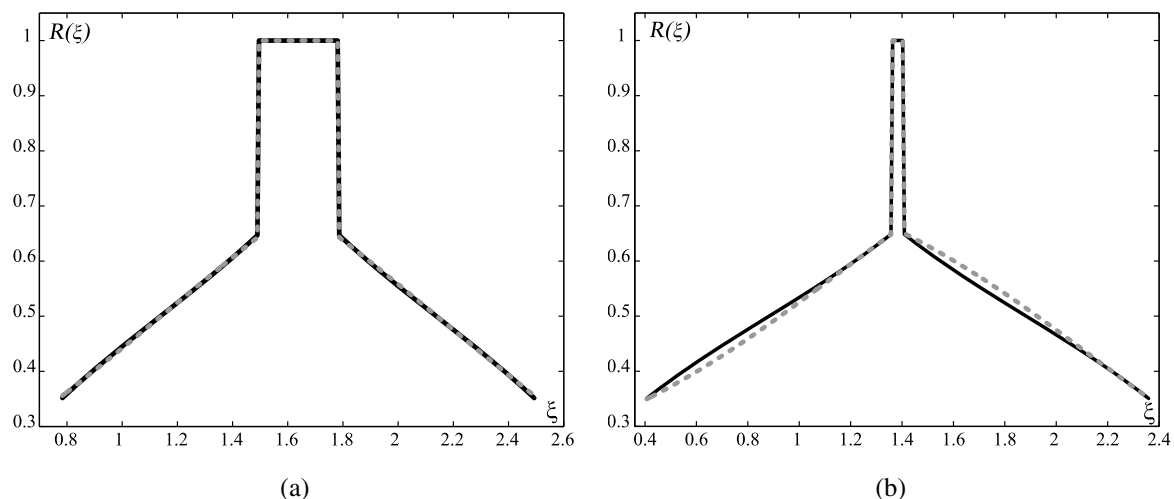


Fig. 14 Numerical (*dashed*) and analytical (*solid*) functions of $R(\xi)$: (a) best fit; (b) worst fit

at one of the limits of the interval of contact, but in this case the opposite limit: the inner point of contact of the pinion.

Several cases have been considered with enlarged addendum: on pinion (Study_2a and Study_2b), on wheel (Study_2c and Study_2d) and on both gears (Study_2e). In these cases, as curves are extended in the extremes, far from the midpoint of the interval of contact, errors increase a little. For enlarged addendum on pinion error increases at the outer point of contact; for enlarged addendum on wheel error increases at the inner point of contact; for enlarged addendum on pinion and wheel error increases at both limits of the in-

terval, as shown in Table 1. Maximum errors also increase because points of maximum error are shifted to the limits of the interval; however error levels remain low enough, in particular for the load sharing ratio. R^2 factor keeps values between 0.9826 and 0.9995 for the inverse unitary potential $v(\xi)$ and between 0.9875 and 0.9999 for the load sharing ratio $R(\xi)$.

Study_3a and Study_3b show how the tooth dedendum has very small influence on the load sharing ratio, though its influence on the inverse unitary potential is slightly greater.

Finally, Study_4 shows the influence of center distance modifications. In this case, as the center distance

is enlarged, meaning a reduction of the effective contact ratio, errors at the limits or the interval of contact are smaller, while maximum errors are more or less the same as those for standard center distance.

Example An example may illustrate the load calculation of non-standard gears. Consider a non-standard spur gear pair with the following geometrical parameters:

- Number of teeth on pinion: 16
- Gear ratio: 1.5
- Pressure angle: 19 deg
- Rack shift coefficient: 0 (both on pinion and wheel)
- Dedendum coefficient: 1.25
- Addendum coefficient: 1.1
- Operating center distance: $r_{p1} + r_{p2} + 0.1m_n$

The corresponding standard spur gear pair will have the same geometrical parameters, except de addendum coefficient (1.0) and the operating center distance ($r_{p1} + r_{p2}$).

Neglecting possible vacuum gearing effects, the fictitious transverse contact ratio of this standard gear is $\varepsilon'_\alpha = 1.5859$, and the fictitious inner point of contact, is described by $\xi'_{inn} = 0.0559$. From these values, the middle and the outer point of the contact interval are described by:

$$\begin{aligned} \xi'_m &= \xi'_{inn} + \frac{\varepsilon'_\alpha}{2} = 0.8489 \\ \xi'_{out} &= \xi'_{inn} + \varepsilon'_\alpha = 1.6418 \end{aligned} \tag{30}$$

while the coefficient b'_0 is given by:

$$b'_0 = \left[\frac{1}{2} \left(1 + \frac{\varepsilon'_\alpha}{2} \right)^2 - 1 \right]^{-1/2} = 1.2832 \tag{31}$$

The increase of the operating center distance results in a reduction of the fictitious contact ratio of an amount of $(\Delta\varepsilon_\alpha)_c = 0.1013$. The new values of the profile parameters of the inner and middle points of the interval of contact will be:

$$\begin{aligned} \xi''_{inn} &= \xi'_{inn} + (\Delta\varepsilon_\alpha)_c = 0.1572 \\ \xi''_m &= \xi'_m + \frac{(\Delta\varepsilon_\alpha)_c}{2} = 0.8996 \end{aligned} \tag{32}$$

The increase of the pinion addendum increases the transverse contact ratio of an amount of 0.0613, or what is the same, the reduction of the contact ratio is $(\Delta\varepsilon_\alpha)_{out} = -0.0613$. The new outer point of contact is described by:

$$\xi_{out} = \xi'_{out} - (\Delta\varepsilon_\alpha)_{out} = 1.7031 \tag{33}$$

The increase of the wheel addendum produces vacuum gearing at the pinion root, so the inner point of contact will be coincident with the start of involute, which in this case is described by $\xi_{inn} = 0.1113$ [26]. The variation of the transverse contact ratio is described by $(\Delta\varepsilon_\alpha)_{inn} = -0.0459$.

Summarizing the above results, the inverse unitary potential of the studied non-standard spur gear will be given by:

$$\begin{aligned} v(\xi) &= \cos[b'_0(\xi - \xi''_m)] \\ &\text{for } \xi_{inn} \leq \xi \leq \xi_{inn} + \varepsilon_\alpha \\ v(\xi) &= 0 \\ &\text{for } \xi < \xi_{inn} \text{ or } \xi > \xi_{inn} + \varepsilon_\alpha \end{aligned} \tag{34}$$

Here, according to the calculations above, $b'_0 = 1.12832$, $\xi''_m = 0.8996$, $\xi_{inn} = 0.1113$ and the effective transverse contact ratio is:

$$\begin{aligned} \varepsilon_\alpha &= \varepsilon'_\alpha - (\Delta\varepsilon_\alpha)_c - (\Delta\varepsilon_\alpha)_{inn} - (\Delta\varepsilon_\alpha)_{out} \\ &= 1.5918 \end{aligned} \tag{35}$$

The load sharing ratio can be easily computed with Eqs. (9) and (34).

The inverse unitary potential and the load sharing ratio have been also computed by numerical integration of Eqs. (2). Results are shown in Fig. 15. It can be observed the very good fit between the numerical calculations and the presented model. The maximum relative error in the estimation of the inverse unitary potential $v(\xi)$ is 2.64 % (located at $\xi = 0.1733$), and the R^2 -factor is 0.9975. For the load sharing ratio $R(\xi)$ the maximum relative error is 1.56 % (located at the inner point of contact) while de R^2 -factor grows up to 0.9999.

5 Comparison with ISO rating method

Reference [20] presents a complete study on the discrepancies between the ISO rating methods and calculations based on the new model of load distribution of Minimum Elastic Potential (MEP). As ISO [3, 4] neglects the load distribution and use some influence coefficients to correct the simplified calculations based on an even load distribution along the line of contact, comparisons were made throughout the values of the critical contact stress. The results of this comparative study for spur gears can be summarized as follows [20]:

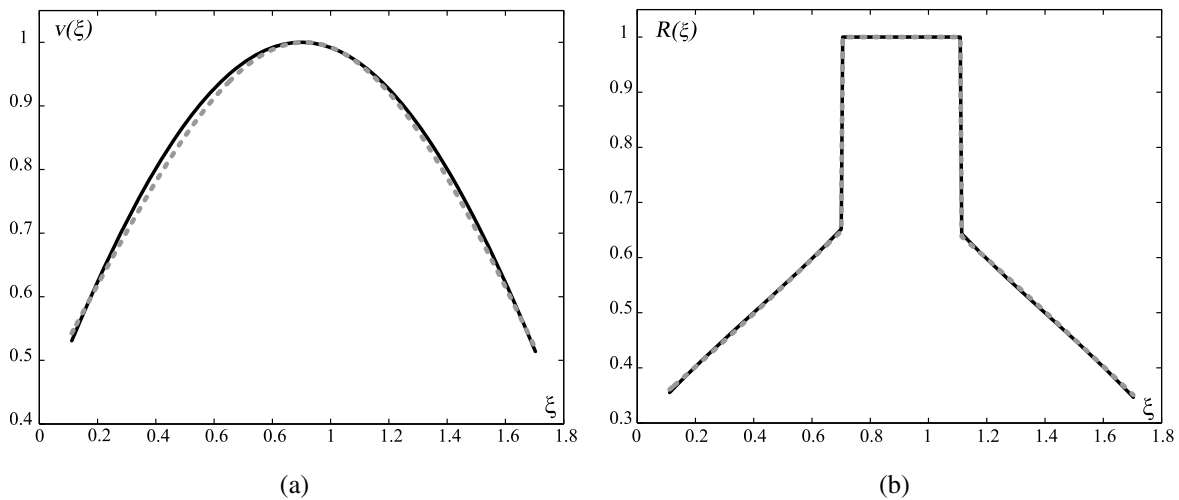


Fig. 15 Comparison between numerical (*dashed*) and analytical (*solid*) calculations of the example: **(a)** inverse unitary potential; **(b)** load sharing ratio

- The critical contact stress is usually located at the inner point of single pair tooth contact, both for ISO and MEP methods. However, results are not identical due to the virtual face with (or the contact ratio factor [3]) considered by ISO. Discrepancies depend on the values of the transverse contact ratio, but typically the ISO contact stress is around 10 % smaller than MEP contact stress.
- For small values of the pinion tooth number, the MEP critical contact stress may be located at the inner point of contact, while the ISO one remains at the inner point of single pair tooth contact. In this case, discrepancies increase up to 35 %, for gear ratio greater than 3.

All these conclusions have been obtained by studying spur gears with standard tooth proportions and standard center distances. ISO calculation methods may not fit accurately to non-standard tooth height or center distance. However, the same rating method can be adapted to non-standard dimensions by considering four possible determinant contact points: both limits of the interval of contact and both limits of the interval of single pair tooth contact (instead of the inner point of contact and the inner point of single pair tooth contact, exclusively [3]). From this assumption, the discrepancies between the ISO rating method and the MEP calculations for non-standard gear dimensions are similar to those for standard gear dimensions, except for critical contact stress located at different contact points, in which discrepancies are not higher than 20 %, much

smaller than 35 % corresponding with standard gears. A new example may be illustrative.

Example One of the gears considered in Study_1c was:

- Number of teeth on pinion: 25
- Gear ratio: 2.0
- Pressure angle: 25 deg
- Rack shift coefficient: 0 (both on pinion and wheel)
- Dedendum coefficient: 1.25
- Pinion addendum coefficient: 1.0
- Wheel addendum coefficient: 0.9
- Operating center distance: $r_{p1} + r_{p2}$

The values of the fictitious contact ratio and the actual contact ratio are:

$$\begin{aligned} \varepsilon'_\alpha &= 1.6385 \\ \varepsilon_\alpha &= 1.5605 \end{aligned} \tag{36}$$

while the values of the profile parameter of the fictitious and actual inner point of contact are:

$$\begin{aligned} \xi'_{inn} &= 0.6756 \\ \xi_{inn} &= 0.7536 \end{aligned} \tag{37}$$

According to Eq. (19),

$$\begin{aligned} \xi'_m &= \xi'_{inn} + \frac{\varepsilon'_\alpha}{2} = 1.4769 \\ b'_0 &= \left[\frac{1}{2} \left(1 + \frac{\varepsilon'_\alpha}{2} \right)^2 - 1 \right]^{-1/2} = 1.2358 \end{aligned} \tag{38}$$

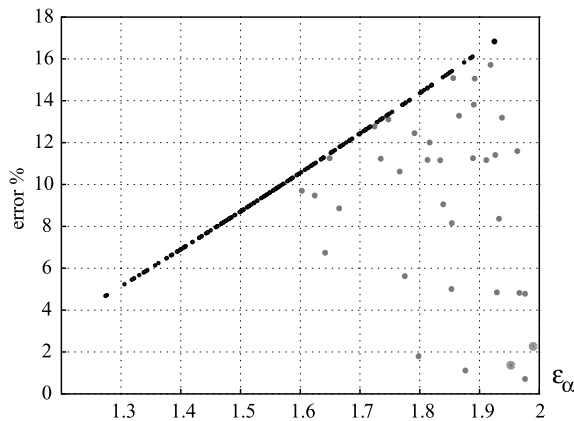


Fig. 16 Comparison between ISO and MEP critical contact stresses

And finally, from Eq. (20), the load sharing ratio is given by:

$$\begin{aligned}
 R(\xi) &= -0.0194 + 0.5221\xi \\
 &\text{for } 0.7536 \leq \xi \leq 1.3114 \\
 R(\xi) &= 1 \\
 &\text{for } 1.3114 \leq \xi \leq 1.7536 \\
 R(\xi) &= 1.5414 - 0.5221\xi \\
 &\text{for } 1.7536 \leq \xi \leq 2.3114
 \end{aligned} \tag{39}$$

From this load distribution, the critical contact stress provided by MEP method is 8.86 % greater than ISO nominal contact stress, both of them computed as described in [3] and [20]. In this case, both methods locate the critical contact stress at the inner point of single pair tooth contact.

Figure 16 presents the discrepancies ISO and MEP critical contact stresses for all the cases of all the studies presented in Table 1. Black points represent the cases in which ISO and MEP critical stresses are both located at the inner point of single pair tooth contact. In these cases, discrepancies arise due to the ISO contact ratio factor [3], and depend on the value of the contact ratio, exclusively. Grey points represent all the other cases, in which the source of the discrepancies is not only the contact ratio factor but also the different critical point—and relative curvature radius—and the different fraction of the load considered by each method.

6 Conclusions

In this paper, a non-uniform model of load distribution along the line of contact of standard spur and helical gears, obtained from the minimum elastic potential criterion, has been enhanced to fit with the meshing conditions of non-standard cylindrical gear pairs, with non-standard values of the tooth height or the center distance, or the presence of undercut at the pinion root. The same analytical formulation of the initial model, based on an approximate equation for the inverse unitary potential, may be used for the non-standard gears by considering appropriate values of the contact ratio and the limits of the interval of contact.

For non-standard tooth height the expression of the inverse unitary potential for the standard height remain valid, except the limits of the interval, according to the new values of the inner and outer points of contact. This means that the curve is the same, with the same equation, but truncated or enlarged at one or both extremes. The presence of vacuum gearing at the pinion root can be considered as a reduction of the wheel tooth height, which means the inverse unitary potential should be truncated at the left side.

For non-standard center distance the equation is also the same as that for standard center distance, but in this case the curve should be truncated (or enlarged) at both sides the same amount, and shifted to ensure the upper limit of the interval of contact keeps its initial value, because the outer point of contact of the pinion does not change.

Developed studies of accuracy reveal that approximate analytical equation of the inverse unitary potential fits very well with values obtained by numerical calculation, also for non-standard gears considered in this work. Typical values of the adjusted R^2 -factor are higher than 0.99 and higher than 0.999 in more than 50 % of the studied cases, but errors are even smaller for the load sharing ratio: adjusted R^2 -factor grows up to 0.999 for more than 75 % of the studied cases, and is always greater than 0.987. Discrepancies with ISO rating method are similar to those for standard gears: MEP contact stress is around 10 % greater than ISO one, both for critical contact stress located at the same contact point or not.

Acknowledgements Thanks are expressed to the Spanish Council for Scientific and Technological Research for the support of the projects DPI2008-05787, “Calculation Models for Special Cylindrical Gears”, and DPI2011-27661, “Advanced

Models for Strength Calculation and Dynamic Analysis of Non-Conventional Cylindrical Gears”.

References

1. AGMA Standard 2001-D04 (2004) Fundamental rating factors and calculation methods for involute spur and helical gear teeth. American Gear Manufacturers Association, Alexandria
2. AGMA Information Sheet 908-B89 (1989) Geometry factors for determining the pitting resistance and bending strength of spur, helical and herringbone gear teeth. American Gear Manufacturers Association, Alexandria
3. ISO Standard 6336-2:2006 (2006) Calculation of load capacity of spur and helical gears—Part 2: Calculation of surface durability (pitting). International Organization for Standardization, Geneva, Switzerland
4. ISO Standard 6336-1:2006 (2006) Calculation of load capacity of spur and helical gears—Part 1: Basic principles, introduction and general influence factors. International Organization for Standardization, Geneva, Switzerland
5. Hayashi K (1963) Load distribution on the contact line of helical gear teeth. *JSME Bull* 22
6. Winter H, Placzek T (1991) Load distribution and topological flank modification of helical and double helical gears. *Eur J Mech Eng* 36(3)
7. Zhang Y, Fang Z (1999) Analysis of tooth contact and load distribution of helical gears with crossed axes. *Mech Mach Theory*. doi:10.1016/S0094-114X(98)00006-8
8. Boerner J (1996) Very efficient calculation of the load distribution on external gear sets—the method and applications of the program LVR. In: Proc. 7th international power transmission and gearing conference, San Diego
9. Ajmi M, Vexlex P (2005) A model for simulating the quasi-static and dynamic behavior of solid wide-faced spur and helical gears. *Mech Mach Theory*. doi:10.1016/j.mechmachtheory.2003.06.001
10. Li S (2008) Effect of addendum on contact strength, bending strength and basic performance parameters of a pair of spur gears. *Mech Mach Theory*. doi:10.1016/j.mechmachtheory.2007.12.010
11. Nicoletto G (1992) Gear tooth stress analysis by the complex potentials method. *Meccanica*. doi:10.1007/BF00420588
12. Arafa MH, Megahed MM (1999) Evaluation of spur gear mesh compliance using the finite element method. *Proc IME C J Mech Eng Sci*. doi:10.1243/0954406991522509
13. Pimsarn M, Kazerounian K (2002) Efficient evaluation of spur gear tooth mesh load using pseudo-interference stiffness estimation method. *Mech Mach Theory*. doi:10.1016/S0094-114X(02)00022-8
14. Nadolski W (1996) Influence of nonlinear stiffness of teeth on dynamic loads in gear transmission. *Meccanica*. doi:10.1007/BF00426973
15. Vedmar L (1981) On the design of external involute helical gears. PhD thesis. Lund Technical University, Lund, Sweden
16. Höhn BR (2010) Improvements on noise reduction and efficiency of gears. *Meccanica*. doi:10.1007/s11012-009-9251-x
17. Pedrero JI, Artés M, Fuentes A (1999) Modelo de distribución de carga en engranajes cilíndricos de perfil de evolvente. *Rev Iberoam Ing Mec* 3(1)
18. Pedrero JI, Pleguezuelos M, Artés M, Antona JA (2010) Load distribution model along the line of contact for involute external gears. *Mech Mach Theory*. doi:10.1016/j.mechmachtheory.2009.12.009
19. Pedrero JI, Vallejo II, Pleguezuelos M (2007) Calculation of tooth bending strength and surface durability of high transverse contact ratio spur and helical gear drives. *J Mech Des*. doi:10.1115/1.2403773
20. Pedrero JI, Pleguezuelos M, Muñoz M (2011) Critical stress and load conditions for pitting calculations of spur and helical gear teeth. *Mech Mach Theory*. doi:10.1016/j.mechmachtheory.2010.12.001
21. Pedrero JI, Pleguezuelos M, Muñoz M (2011) Contact stress calculation of undercut spur and helical gear teeth. *Mech Mach Theory*. doi:10.1016/j.mechmachtheory.2011.06.015
22. Pedrero JI, Estrems M, Fuentes A (1999) Determination of the efficiency of cylindrical gear sets. In: Proc. IV world congress on gearing and power transmissions, Paris, France, vol 1
23. Pedrero JI, Pleguezuelos M, Muñoz M (2009) Simplified calculation method for the efficiency of involute spur gears. In: Proc. ASME IDETC/CIE 2009, San Diego
24. Pleguezuelos M, Pedrero JI, Sánchez MB (2010) Simplified calculation method for the efficiency of involute helical gears. In: New trends in mechanism science, Cluj-Napoca, Romania
25. Borelli AP, Sidebottom OM, Seely FB, Smith JO (1978) *Advanced mechanics of materials*. Wiley, New York
26. Pedrero JI, Artés M, García-Masiá C (2004) Determination of the effective path of contact of undercut involute gear teeth. *J Mech Eng Sci*. doi:10.1243/0954406041319464